

RSC Advances



This is an *Accepted Manuscript*, which has been through the Royal Society of Chemistry peer review process and has been accepted for publication.

Accepted Manuscripts are published online shortly after acceptance, before technical editing, formatting and proof reading. Using this free service, authors can make their results available to the community, in citable form, before we publish the edited article. This *Accepted Manuscript* will be replaced by the edited, formatted and paginated article as soon as this is available.

You can find more information about *Accepted Manuscripts* in the [Information for Authors](#).

Please note that technical editing may introduce minor changes to the text and/or graphics, which may alter content. The journal's standard [Terms & Conditions](#) and the [Ethical guidelines](#) still apply. In no event shall the Royal Society of Chemistry be held responsible for any errors or omissions in this *Accepted Manuscript* or any consequences arising from the use of any information it contains.

- 23 Email Addresses:
- 24
- 25 Hua Zhong: zhonghua@email.arizona.edu
- 26 Lei Yang: wlwyanglei@126.com
- 27 Xin Yang: yx2013@hnu.edu.cn
- 28 Guangming Zeng: zgming@hnu.edu.cn
- 29 Zhifeng Liu: lzf18182002@163.com
- 30 Yang Liu: liuyang_feiyang@163.com
- 31 Xingzhong Yuan: yxz@hnu.edu.cn

32 **Abstract:**

33 Dynamic light scattering (DLS) and cryo-transmission electron microscopy
34 (Cryo-TEM) tests demonstrated aggregate formation for dirhamnolipid biosurfactant
35 (diRL) at concentrations lower than surface-tension-based critical micelle
36 concentration (CMC_{st}). Increase of diRL concentration and solution pH results in
37 decrease of the aggregate size at diRL concentration below CMC_{st} , whereas it has no
38 influence at diRL concentration above CMC_{st} . The cryo-TEM micrographs show
39 spherical morphology of aggregates, and logarithm of aggregate size follows Gaussian
40 distribution. The aggregates are negatively charged. Zeta potential of the aggregates
41 decreases with increase of diRL concentration to CMC_{st} , and stabilizes at diRL
42 concentrations higher than CMC_{st} . Increase of solution pH causes decrease of zeta
43 potential. A transitional state assumption is raised for interpretation of the diRL
44 aggregation behavior. The results demonstrate formation of aggregates at significantly
45 low diRL concentrations, which is of importance for cost-effective application of
46 rhamnolipid biosurfactant.

47 **Keywords:** dirhamnolipid; aggregation; critical micelle concentration; zeta potential.

48 **1 Introduction**

49 Biosurfactants are surfactants produced by microbes. Due to expanding
50 application of biosurfactants in many fields, e.g. biomedicine and bioremediation,
51 their aggregation behaviour in electrolyte has received much attention in recent years.
52 ¹⁻³ The aggregates have a variety of microstructures, including spherical, globular or
53 cylindrical micelles, ^{1,4-8} spherical or irregular vesicles, ^{2,9,10} tubular or irregular
54 bilayers, ¹¹ and lamellar sheets. ^{3,12,13} Also, the lyotropic liquid crystalline phases with
55 lamellar, hexagonal and cubic aggregate morphologies are observed at high surfactant
56 concentrations¹⁴. The morphology of these aggregates has been demonstrated to be
57 affected by surfactant concentration, ^{8,15} pH, ^{4,10,16} temperature, ¹² counterions, ^{1,10,15} and
58 ionic strength.¹⁷

59 Rhamnolipid is the most widely studied biosurfactant and its aggregates exhibit
60 versatile structures at concentrations higher than the critical micelle concentration
61 (CMC). For example, Ishigami et al. investigated the effect of solution pH on
62 rhamnolipid aggregate structure at concentrations of 500-20000 mg/L in phosphate
63 buffered saline solution. The result showed that the aggregates existing in form of
64 bilayers vesicle at pH of 4.3-5.8, bilayer lamella with pH rising to 6.0-6.5, and
65 micelles with further increase of pH to 6.8.¹⁸ Champion et al. determined the
66 rhamnoliopid aggregate morphology at various pH at the concentration of 60 mM by
67 Cryo-TEM. The results show that aggregate phase transitioned in an order of bilayer
68 lamella, large vesicles, small vesicles and micelle with the increase of pH.⁴ In

69 addition, transformation of dirhamnolipid aggregations from large particles into small
70 particles with the increase of concentration at fixed pH has also been reported.¹⁹

71 All these prior researches, however, were almost implemented with surfactant
72 concentrations far higher than CMC. However, there are studies showing that
73 rhamnolipid exhibited excellent HOC-solubilization activity at significantly low
74 concentrations. For example, rhamnolipid can enhance the solubility of hexadecane
75 and octadecane by 3~4 orders of magnitude at concentrations lower than CMC
76 determined by surface tension method, and such solubilization efficiency is much
77 higher than at concentrations above CMC.^{16,20} Hypothetically these
78 HOC-solubilization activities of rhamnolipid surfactant may be related to its
79 aggregation behavior at low concentrations, e.g. lower than CMC. Furthermore, signs
80 of aggregate formation at concentrations lower than CMC for multi-component
81 rhamnolipids were observed using dynamic lighter scattering method.^{7,15} Formation
82 of premicelles for a variety of surfactants also have been reported.²¹⁻²⁴ These
83 observations indicate the probability of sub-CMC aggregate formation for
84 rhamnolipid, which still remains unexplored.

85 In this study, the aggregation behavior of dirhamnolipid in phosphate buffered
86 electrolyte solution with concentrations near surface-tension-based CMC (or CMC_{st})
87 was investigated. The objective of this study is to examine whether rhamnolipid forms
88 aggregate at concentrations below CMC_{st} , and to explore the effect of solution
89 conditions on aggregate formation at low rhamnolipid concentration range.

90

91 **2 Materials and methods**

92 **2.1 Biosurfactant and chemicals**

93 The dirhamnolipid biosurfactant was produced, extracted, purified, and
94 characterized using the method described by Zhong et al.²⁵ NaOH and HCl (analytical
95 chemistry grade) were purchased from Damao Chemical (Tianjin, China). All other
96 chemicals (NaNO_3 , KH_2PO_4 , $\text{Na}_2\text{HPO}_4 \cdot 12\text{H}_2\text{O}$, MgSO_4 , $\text{FeSO}_4 \cdot 7\text{H}_2\text{O}$) were
97 analytical chemistry grade with purity > 99% and purchased from Sinopharm (Beijing,
98 China).

99 **2.2 Determination of CMC_{st}**

100 The stock solution of the diRL were prepared in phosphate buffered saline
101 solution (PBSS, NaNO_3 2g/L, KH_2PO_4 1.5g/L, $\text{Na}_2\text{HPO}_4 \cdot 12\text{H}_2\text{O}$ 1.5g/L, MgSO_4
102 0.1g/L, $\text{FeSO}_4 \cdot 7\text{H}_2\text{O}$ 0.01g/L). PBSS solutions of diRL in a series of concentrations
103 were prepared using dilution method. Surface tension of diRL solutions was measured
104 at 30°C with surface tensiometer (JZ-200A, Chengde, China) using the Du Noüy
105 Ring method. CMC_{st} of diRL was obtained from the relation of surface tension and
106 diRL concentration using the scheme described by Yuan et al.²⁶ Electrical
107 conductivity of diRL solutions was measured with DDS-11A Conductivity Meter
108 (Shengci, Shanghai, China).

109 **2.3 Hydrodynamic aggregate size and zeta potential.**

110 pH of PBSS solutions of diRL was adjusted to 8.0 with 20% NaOH solution
111 using a capillary glass pipe. High concentration of NaOH was used to minimize
112 change of solution volume during pH adjustment. These solutions were then filtered

113 through a 0.22 μm filter (Millex-HV, Millipore, Billerica, Ma, US) to remove
114 suspended solid particles that may interfere with the measurement. Results of
115 preliminary test showed that the size of rhamnolipid aggregates is far less than
116 0.22 μm at pH 8.0, so they will not be retained by filtering. The solutions were
117 allowed to stand still for 2 h. Then pH of the solutions was adjusted in sequence to
118 7.5, 7.0, 6.5, or 6.0 with 20% hydrochloric acid. For each sample, aggregate size and
119 zeta potential were measured using Zetasizer Nano ZEN3600 (Malvern Instruments,
120 U.K.).

121 The aggregate particle size was determined based on dynamic light scattering
122 (DLS) mechanism using He-Ne laser at wavelength of 623nm and working power of
123 4.0 mW. 1 ml of the sample was loaded to the DTS-0012 cell and measured at
124 temperature of 30°C. The scattered light was collected by receptor at angle of 173°
125 from light path. A mean size provided by DTS Nano software (Malvern Instruments,
126 U.K.) was used to represent the aggregate size of the sample. Also, the number-based
127 particle size distribution (number PSD) data generated by the software were used for
128 the statistical analysis of aggregate size.

129 The zeta potential measurement is based on the mechanism of particle
130 electrophoresis in aqueous solution. 1 mL sample is loaded to DTS 1060 folded
131 capillary cell and the electrophoretic mobility of the aggregate was measured at 30°C
132 under automatic voltage using a laser Doppler velocimetry with M3-PALS technique
133 to avoid electroosmosis. The measured data was converted into corresponding zeta
134 potential by applying the Helmholtz-Smoluchowski equation.²⁷

135 **2.4 Cryo-Transmission electron microscopy test.**

136 DiRL solution or electrolyte solution in the absence of diRL in volume of 4uL
137 was placed on the grid with a holy polymer film using a microsyringe, and then sent
138 to a FEI Vitrobot sample plunger system (FEI, Hillsboro, Oregon). Excessive sample
139 was removed by a filter paper. Then the sample grid was rapidly vitrified in liquid
140 ethane and transferred to a liquid nitrogen bath. The morphology of diRL aggregate
141 were then viewed and photographed on a Tecnai F20 Transmission Electron
142 Microscope (FEI, Hillsboro, Oregon) at an acceleration voltage of 120 kV. Nano
143 measurer 1.2.5 software (Shanghai, Fudan University) was used to process the
144 micrograph images. The program marked the recognized particles in an image with
145 circles. The diameter of every circle was measured by pairing the circle to a screen
146 ruler calibrated by the reference bar in the image and used as the size of the particle.
147 In order to obtain statistically representative sample for aggregate size distribution
148 analysis, the size data were collected on more than 100 or 200 particles from multiple
149 images for rhamnolipid concentrations of 25 or 250 μM , respectively.

150

151 **3 Results and Discussion**

152 For all the pHs, surface tension of the solution decrease significantly with the
153 increase of rhamnolipid concentration at low surfactant concentrations, and then
154 further increase of surfactant concentration has no significant effect on surface tension
155 (Fig. 1). Based on the method of Yuan et al.,²⁶ the CMC_{st} values obtained are 62, 78,
156 82, 83 and 82 μM for pH of 6.0, 6.5, 7.0, 7.5 and 8.0, respectively. The result showed

157 that the increase of solution pH resulted in increase of diRL CMC_{st} for pH not higher
158 than 7.0. The electrical conductivity of diRL solution increased with the increase of
159 diRL concentration for all pH conditions, however, the two-line profile with a
160 distinguishable slope inflection is not observed for any of the curves (Fig. S1a, SI).
161 The plot of conductivity derivative versus diRL concentration is presented in Fig.
162 S1b, SI. The conductivity derivative shows a gradual decrease at the concentration
163 below CMC_{st} , which is in contrast to an abrupt decrease at CMC general for regular
164 surfactants.

165 Results of DLS-size measurement show that diRL aggregates were detected at
166 diRL concentration both below and above CMC_{st} . The number PSD profiles generated
167 by Malvern DTS Nano software show only one peak for all the conditions of
168 measurements (typical profiles are presented in Fig. S2, SI), indicating presence of
169 only one type of aggregate. The influence of diRL concentration and solution pH on
170 aggregate size is shown in Fig. 2a. The aggregate size is in a range of 8 to 72 nm.
171 When the solution pH is not higher than 7.0, the aggregate size decreased with the
172 increase of diRL concentration up to 100 μM . At diRL concentrations ranging from
173 10 to 100 μM (close to CMC_{st}), the aggregate size decreases rapidly with increase of
174 pH. When diRL concentration is higher than 100 μM , both diRL concentration and
175 pH have no observable influence on the aggregate size. The relation between DLS
176 diffusion coefficients and diRL concentrations is shown in Fig. S3, SI. The diffusion
177 coefficient increases with increase of diRL concentration when the concentration is
178 lower than CMC_{st} . This result is in contrast to DLS diffusion coefficient for regular

179 surfactants, for which an abrupt decrease of the coefficient is observed at CMC.²⁸
180 This result, however, matches with the result of size measurement in that diffusion
181 coefficient is larger for smaller particles.

182 Aggregate zeta potential variation with diRL concentration and pH is presented
183 in Fig. 2b. Because rhamnolipid is an anionic surfactant with carboxyl group in the
184 hydrophilic moiety of the molecule, dissociation of the carboxyl groups yields
185 negatively-charged aggregate surface and hence negative zeta potential of the
186 aggregates. For all the pHs, the zeta potential decreases significantly the increase of
187 diRL concentration from 25 μM to 100 μM . Further increase of concentration has
188 minimal influence. For all the diRL concentrations tested, increase in solution pH
189 causes decrease in aggregate zeta potential. Increase of solution pH results in
190 enhanced dissociation of diRL carboxyl group, which in turn increases the aggregate
191 surface charge density and lowers zeta potential (provided a dissociation equilibrium
192 constant of $10^{-5.6}$ for rhamnolipid carboxyl group at room temperature,¹⁸ the
193 dissociation rate of the rhamnolipid is 71.5, 88.8, 96.2, 98.8, 99.6% at pH of 6.0, 6.5,
194 7.0, 7.5, 8.0, respectively).

195 25 μM (below CMC_{st}) and 250 μM (above CMC_{st}) of diRL solution at pH of 6.0
196 or 8.0 were examined using cryo-TEM. Typical images of the aggregates are
197 presented in Fig. 3. Aggregates are observed for all the four conditions, which is in
198 contrast to the observation in the absence of diRL for which no aggregates are
199 observed (Fig. S4a, SI). The morphology of the aggregates is spherical with minimal
200 transparency, indicating micelle-type structure. Other aggregate structures reported in

201 literatures at relatively high rhamnolipid concentrations, e.g. vesicles, lamella or
202 microtubes,^{4,8,9,19} are not observed for any of the conditions tested. This is consistent
203 with the result of DLS size measurement that only one type of aggregate is observed.
204 The cryo-TEM result further confirms formation of diRL aggregates at concentrations
205 below CMC. On the other hand, the DLS size and cryo-TEM results also shows that
206 the aggregates are not premicelles, which are defined as dimers and low-aggregation
207 number aggregates of surfactant molecules before micelle formation.²¹⁻²⁴

208 All the cryo-TEM images used for aggregate size distribution analysis are shown
209 in Fig. S4, SI. Gaussian distribution is commonly used to depict natural phenomena
210 associated with real-valued random variables whose distributions are unknown. The
211 distributions of aggregate sizes obtained with either DLS or cryo-TEM method appear
212 to deviate from Gaussian distribution (data not shown), however, natural logarithm of
213 the sizes follows Gaussian distribution very well for all the four conditions examined
214 (Fig. 3). Values of the parameters for the fit are presented in Table 1. The mean of
215 cryo-TEM size at diRL concentration of 25 μM (lower than CMC_{st}) is larger than at
216 diRL concentration of 250 μM (higher than CMC_{st}), for pH of either 6.0 or 8.0. The
217 cryo-TEM size at diRL concentration of 25 μM is larger for pH 6.0 than for pH 8.0,
218 and they are identical at diRL concentration of 250 μM . These results show that
219 change of the cryo-TEM size is similar to that of DLS size in terms of trend,
220 indicating good consistency. The cryo-TEM sizes obtained at the condition of 25 μM
221 diRL and pH 6.0 (24.9 nm) is significantly smaller than the DLS-based size (43.2 nm).
222 The particle size obtained by DLS method is hydrodynamic diameter, which is the

223 diameter of a sphere that has the same translational diffusion coefficient as the particle.
224 This hydrodynamic size is usually larger than the real particle size.²⁹ Either the DLS
225 size or the cryo-TEM size obtained at high diRL concentration (0.5mM) in our study
226 is smaller than that measured at similar concentrations using similar methods in the
227 study of Guo and Hu,⁸ in which formation of large vesicles was observed. The ionic
228 strength of diRL solution in that study is approximately 10 mM, which is significantly
229 lower than that in our study (55 mM with divalent ions). The hydrophilic head of
230 diRL molecule contains a carboxylic group. At pH higher than 6.0, the majority of
231 carboxylic groups are dissociated and negatively charged. Cations in the diRL
232 electrolyte solution can easily bind with the carboxylate groups, resulting in the
233 induction of the solvated groups and disfavours formation of large aggregates.⁹ Such a
234 conversion of large vesicles to small ones was also observed when Cd^{2+} was
235 introduced in solution of rhamnolipid solution.⁴ In addition, the dirhamnolipid used in
236 the study of Guo and Hu contains higher ratio of long-chain species ($\text{Rha}_2\text{C}_{10}\text{C}_{12:1}$ and
237 $\text{Rha}_2\text{C}_{10}\text{C}_{14:1}$. $\text{Rha}_2\text{C}_x\text{C}_{y(z)}$ designates the diRL homologue with x and y as the carbon
238 atom number of each aliphatic acid chain in the lipid moiety, and z as the number of
239 unsaturated bonds in lipid moiety),⁸ which results in stronger hydrophobic interaction
240 between molecules and thus favours formation of large vesicles.

241 The diRL used in this study is not a pure compound comprising one species of
242 molecules. Instead, it is a rhamnolipid mixture consisting of three homologues which
243 are the same in structure of polar moiety (double rhamnose rings and a carboxylic
244 group) while different in length of aliphatic chains ($\text{Rha}_2\text{C}_{10}\text{C}_{10}$, $\text{Rha}_2\text{C}_{10}\text{C}_{12:1}$ and

245 Rha₂C₁₀C₁₂ with molar fractions of 0.70, 0.11 and 0.19, respectively).²⁵ We speculate
246 that this multi-component nature of the diRL results in formation of aggregates at
247 concentrations below CMC_{st}. The strength of hydrophobic interactions between diRL
248 molecules with aliphatic chains of different lengths are not uniform, which may result
249 in a transitional state for aggregation-related behavior, e.g. formation of aggregates in
250 electrolyte solution before the solution surface is saturated with diRL (corresponding
251 to diRL concentration of CMC_{st}) and graduality in change of electrical conductivity
252 increasing rate. In the transitional state, increase in diRL solution concentration may
253 enhance partition of diRL molecules to aggregates and therefore increase the density
254 of the molecules in aggregate. Increase of solution pH results in enhanced dissociation
255 of diRL molecules. Both effects enhance the electrostatic repulsion between polar
256 moieties of diRL molecules in aggregates and hence the curvature of aggregates. As a
257 result, when diRL concentrations are lower than CMC_{st} (the transitional state) the
258 aggregate size decreases with increase of the concentration and solution pH.

259

260 **4 Conclusions**

261 DLS and Cryo-TEM methods were used to study aggregation behavior of
262 low-concentration diRL and the results demonstrated formation of aggregates at
263 concentrations below CMC_{st}. The effect of diRL concentration and solution pH on
264 aggregate size and zeta potential is significant when diRL concentration is lower than
265 the CMC_{st}. The multicomponent nature of the diRL and consequently a transitional
266 state are supposed to be responsible for these aggregation behaviors at low diRL

267 concentrations. Also, results of the study indicate that the surface-tension-based CMC
268 may not be used as the concentration defining aggregate formation for
269 multicomponent biosurfactants. This work is of importance for cost-effective
270 application of rhamnolipid. Further researches should be focused on validating the
271 transitional state speculation and characterizing the rhamnolipid aggregates in
272 transitional state in more detail.

273

274 **Supplementary Information**

275 Electrical conductivity versus diRL concentration profile, typical number PSD
276 profiles generated by Malvern DTS Nano software, DLS diffusion coefficient versus
277 diRL concentration profile, and the cryo-TEM images used for aggregate size
278 distribution analysis are included in SI.

279

280 **Acknowledgements**

281 The authors thank National Laboratory for physical sciences, University of
282 Science and Technology of China, for implementing cryo-TEM tests. This study was
283 funded by the National Natural Science Foundation of China (51378192, 51378190,
284 51308200 and 21276269).

285

286 **References**

- 287 1 K. Matsuoka, K. Takagi and C. Honda, *Chem. Phys. Lipids*, 2013, **172**, 6-13.
- 288 2 J. Arutchelvi, J. Sangeetha, J. Philip and M. Doble, *Colloids Surf. B*, 2014, **116**,
289 396-402.
- 290 3 X. Dai, H. Ding, Q. Yin, G. Wan, X. Shi and Y. Qiao, *J. Mol. Graphics*
291 *Modell.*, 2015, **57**, 20-26.
- 292 4 J. T. Champion, J. C. Gilkey, H. Lamparski, J. Retterer and R. M. Miller, *J Colloid*
293 *Interf. Sci.* , 1995, **170**, 569-574.
- 294 5 D. Song, Y. Li, S. Liang and J. Wang, *Colloids Surf. A*, 2013, **436**, 201-206.
- 295 6 M. Chen, C. Dong, J. Penfold, R. K. Thomas, T. J. Smyth, A. Perfumo, R.
296 Marchant, I. M. Banat, P. Stevenson, A. Parry, I. Tucker and I. Grillo, *Langmuir*,
297 2013, **29**, 3912-3923.
- 298 7 H. Abbasi, K. A. Noghabi, M. M. Hamed, H. S. Zahiri, A. A. Moosavi-Movahedi,
299 M. Amanlou, J. A. Teruel and A. Ortiz, *Colloids Surf. B*, 2013, **101**, 256-265.
- 300 8 Y. P. Guo, and Y. Y. Hu, *Colloids Surf. A*, 2014, **445**, 12-20.
- 301 9 O. Pornsunthorntawe, S. Chavadej and R. Rujiravanit, *Colloids Surf. B*, 2009, **72**, 6
302 -15.
- 303 10 Z. A. Raza, Z. M. Khalid, M. S. Khan, I. M. Banat, A. Rehman, A. Naeem and M.
304 T. Saddique, *Biotechnol. Lett.*, 2010, **32**, 811-816.

- 305 11 E. Haba, A. Pinazo, R. Pons, L. Perez and A. Manresa, *Biochim. Biophys. Acta*,
306 *Biomembr.*, 2014, **1838**, 776-783.
- 307 12 Ş. Ş. Helvacı, S. Peker and G. Özdemir, *Colloids Surf. B*, 2004, **35**, 225-233.
- 308 13 W. Worakitkanchanakul, T. Imura, T. Fukuoka, T. Morita, H. Sakai, M. Abe, R.
309 Rujiravanit, S. Chavadej, H. Minamikawa and D. Kitamoto, *Colloids Surf. B*, 2008,
310 **65**, 106-112.
- 311 14 P. K. Vinson, Y. Talmon and A. Walter, *Biophys. J.*, 1989, **56**, 669.
- 312 15 Y. P. Guo, Y. Y. Hu, R. R. Gu and H. Lin, *J. Colloid Interface Sci.*, 2009, **331**,
313 356-363.
- 314 16 Y. M. Zhang and R. M. Miller, *Appl. Environ. Microb.*, 1992, **58**, 3276-3282.
- 315 17 M. Hofer, R. Y. Hampton, C. R. Raetz and H. Yu, *Chem. Phys. Lipids.*, 1991, **59**,
316 167-181.
- 317 18 Y. Ishigami, Y. Gama, H. Nagahora, M. Yamaguchi, H. Nakahara and T. Kamata,
318 *Chem. Lett.*, 1987, **16**, 763-766.
- 319 19 M. Sánchez, F. J. Aranda, M. J. Espuny, A. Marqués, J. A. Teruel, Á. Manresa and
320 A. Ortiz, *J. Colloid Interface Sci.*, 2007, **307**, 246-253.
- 321 20 H. Zhong, Y. Liu, Z. F. Liu, Y. B. Jiang, F. Tan, G. M. Zeng, X. Z. Yuan, M. Yan
322 and Q. Y. Niu, *Int. Biodeter. Biodegr.*, 2014, **94**, 152-159.
- 323 21 L. D. Song and M. J. Rosen, *Langmuir*, 1996, **12**, 1149-1153.

- 324 22 K. Tsubone, Y. Arakawa and M. J. Rosen, *J. Colloid Interface Sci.*, 2003, **262**,
325 516-524.
- 326 23 Q. Miao, Y. Jin, Y. Dong, Z. F. Cao and B. Zhang, *J. Poly. Res.*, 2010, **17**,
327 911-921.
- 328 24 D. N. LeBard, B. G. Levine, R. DeVane, W. Shinoda and M. L. Klein, *Chem. Phys.*
329 *Lett.*, 2012, **522**, 38-42.
- 330 25 H. Zhong, G. M. Zeng, J. X. Liu, X. M. Xu, X. Z. Yuan, H. Y. Fu, G. H. Huang, Z.
331 F. Liu and Y. Ding, *Appl. Microbiol. Biot.*, 2008, **79**, 671-677.
- 332 26 X. Z. Yuan, F. Y. Ren, G. M. Zeng, H. Zhong, H. Y. Fu, J. Liu and X. M. Xu, *Appl.*
333 *Microbiol. Biot.*, 2007, **76**, 1189-1198.
- 334 27 R. J. Zamoski, *Springer Netherlands*, 2008, pp. 841-845.
- 335 28 B. Das, B. maitra, S. M. Mercer, M. Everist and D. G. Leaist, *Phys. Chem. Chem.*
336 *Phys.*, 2008, **10**, 3083-3092
- 337 29 S. Pabisch, B. Feichtenschlager, G. Kickelbick and H. Peterlik, *Chem. Phys. Lett.*,
338 2012, **521**, 91-97.
- 339

Table 1 Gaussian regression parameters for DLS and cryo-TEM aggregate size distribution.

diRL Sample	DLS				cryo-TEM			
	μ^a	$\sigma^2{}^b$	R ²	d^c (nm)	μ	σ^2	R ²	d (nm)
25 μ M,pH 6.0	3.77	0.031	1.00	43.2	3.22	0.033	0.96	24.9
250 μ M,pH 6.0	2.05	0.030	0.97	7.8	2.61	0.053	0.98	13.7
25 μ M,pH 8.0	2.80	0.046	0.98	16.5	3.05	0.033	0.97	21.2
250 μ M,pH 8.0	2.06	0.027	0.98	7.8	2.61	0.044	1.00	13.6

^a mean of $\ln d$ obtained from Gaussian regression

^b variance of $\ln d$ obtained from Gaussian regression

^c the mean aggregate size obtained using $d = e^\mu$

Fig. 1 Surface tension versus diRL concentration in PBSS solution and determination of CMC_{st} .

Fig. 2 DLS size (a) and zeta potential (b) of aggregates as a function of diRL concentration and solution pH.

Fig. 3 Distribution of diRL aggregate size obtained using DLS and cryo-TEM methods and representative Cryo-TEM micrographs of diRL aggregates formed in PBSS solution. (a) 25 μ M, pH 6.0; (b) 250 μ M, pH 6.0 ; (c) 25 μ M, pH 8.0; (d) 250 μ M, pH 8.0.

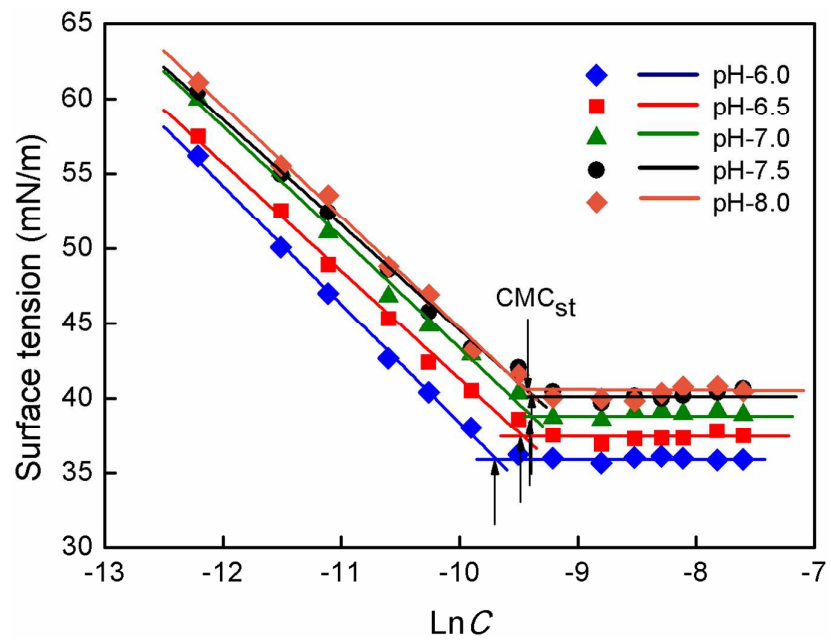


Figure 1

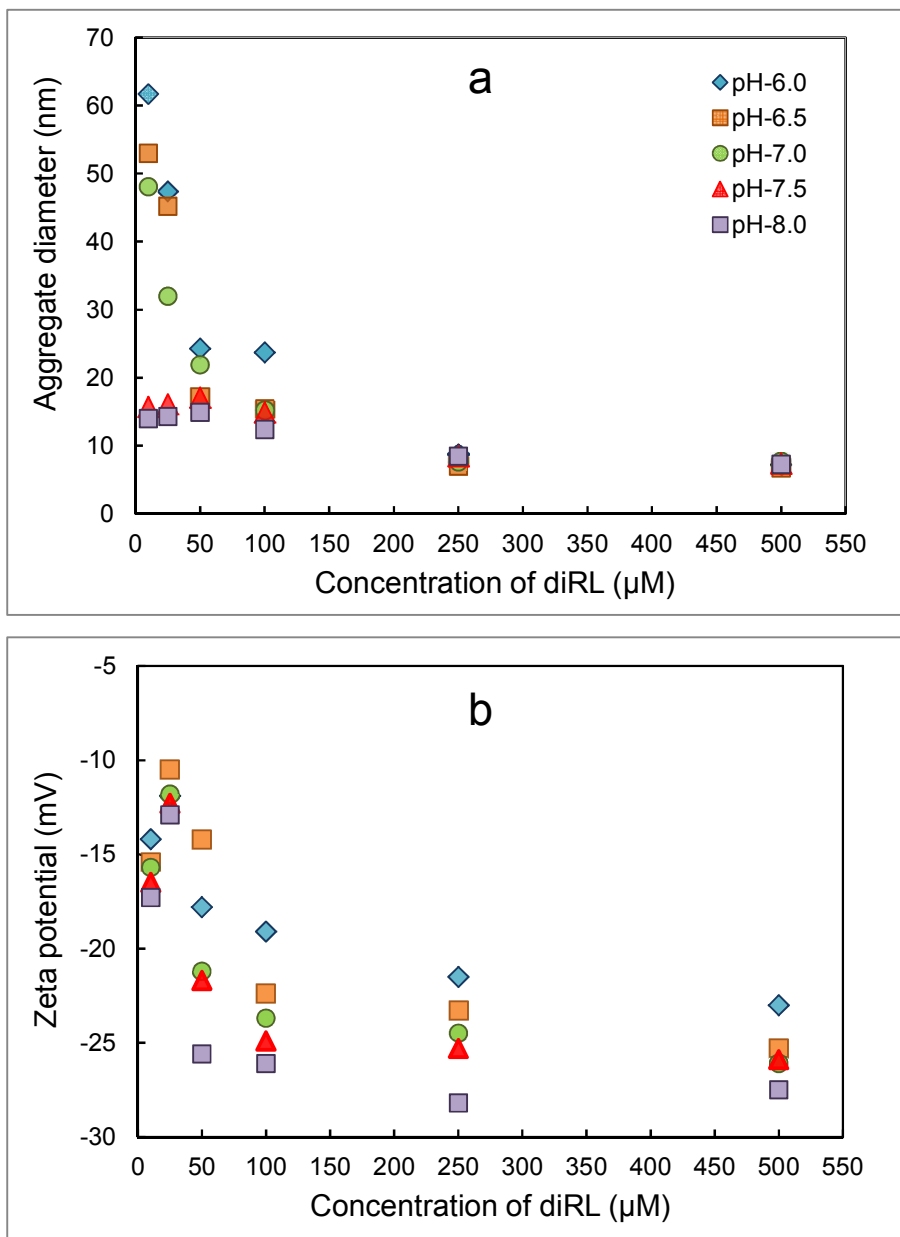
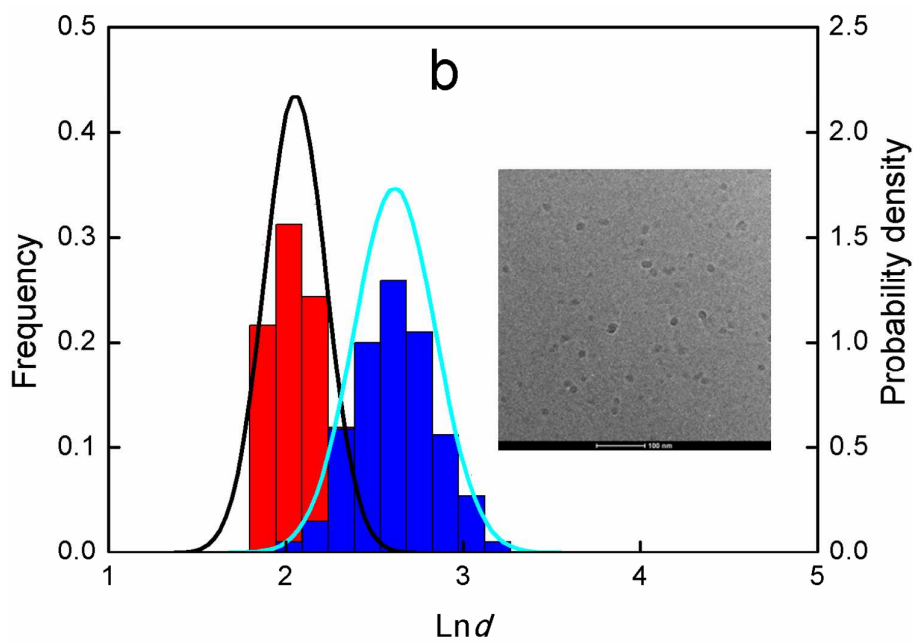
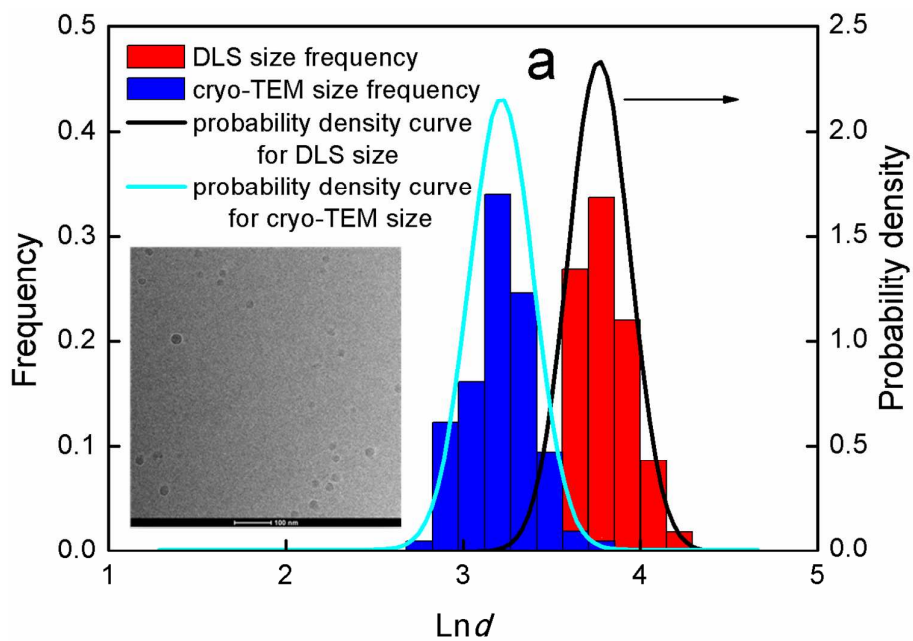


Figure 2



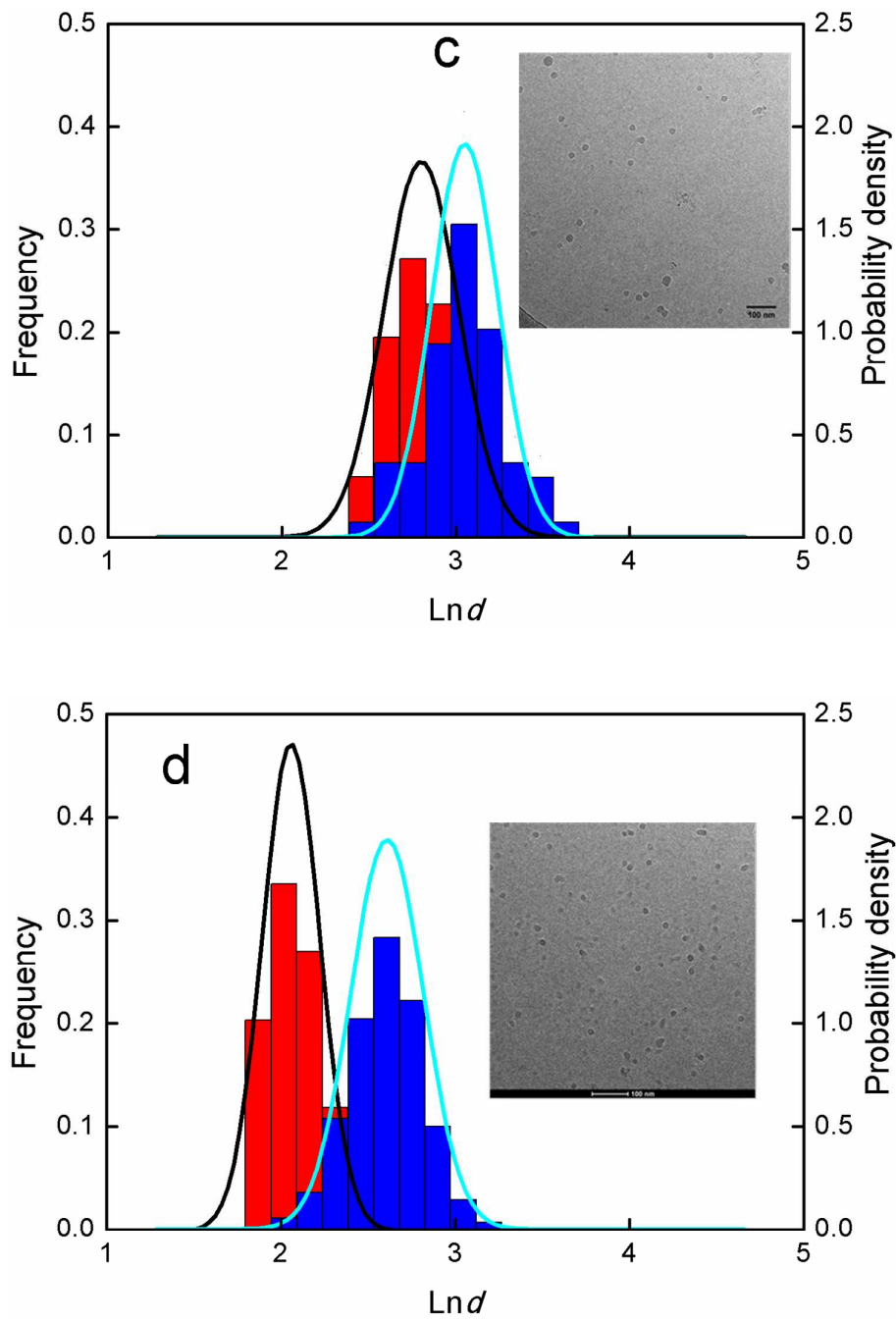


Figure 3